IMPURITY AND DEFECT CHARACTERIZATION IN SILICON

A. Rohatgi, Z. Chen, W.A. Doolittle, J. Salami, and P. Sana

Final Technical Report

October 1, 1991 to March 1992

National Renewable Energy Laboratory

Contract No. XX-0-19145-1

GEORGIA INSTITUTE OF TECHNOLOGY
SCHOOL OF ELECTRICAL ENGINEERING
ATLANTA, GA 30332

TABLE OF CONTENTS

1.

Presence of impurities and crystal defects in the substrate can strongly influence the characteristics of electronic devices. A knowledge of such effects can play a vital role in selection of a substrate of suitable parameters as well as in process designs. This is particular important for fabrication of high efficiency solar cells in low cost silicon substrate such as those obtained by casting and /or as ribbons. Although a wealth of information has already been acquired regarding the influence of some non-dopant impurities on the carrier lifetime in high quality single crystal (such as float zone) silicon substrates, there is relative little meaningful data available on the synergistic effects of impurities and defects on minority carrier lifetime in silicon material and on device parameters. Understanding of such effects is necessary to improve the quality of as grown low-cost silicon substrate as well as developing post-growth processing procedures which can, concomitantly, lead to better cell performance.

Several research groups are investigating impurity-defect issues in silicon substrates for solar cells including: (i) kinetics of defects associated with high speed growth; (ii) influence of thermal treatments on the defect dynamics; (iii) interactions between impurities and defects; and (iv) passivation of impurity/defect "activities". Since impurities play an important role in all these processes it is essential to carry out detailed analysis of the state of impurities in such substrates before and after various process steps. Such detailed information on changes in the defect and impurity concentrations and states needs to be applied, in conjunction with other data from electrical analyses, to develop suitable models which can predict changes in the photovoltaic parameters caused by post-growth processing parameters.

The main objective of this research was to carry out an in-depth impurity analysis

of polycrystalline samples, using techniques such as DLTS, FTIR, and light and dark I-V and correlate their effects on the photovoltaic parameters. The second object of this research was to understand the role of defect and gettering in polycrystalline silicon and develop processes for fabricating high efficiency polycrystalline cells using conventional process sequence and provide silicon solar cell to NREL for optically processed metallization.

In the first annual report (Oct, 1989 - Oct, 1990) of this contract we showed characterization of impurity and defects in Solarex polycrystalline cast silicon and their correlation with cell performance, along with the fabrication and analysis of 15 % efficient polycrystalline silicon solar cells. This report summarizes the work done during Oct 1991 - March 1992. The technical progress in this report is divided into four sections. First section (Chapter 2) explores the potential of poly-Si under high level illumination (> 10 Suns) by a combination of grain boundary and device modeling. Quantitative analysis of the effect of illumination level on grain boundary potential, the minority carrier diffusion length, and cell efficiency is conducted. In chapter 3, PECVD silicon nitride thin films were deposited for AR coating. PECVD produces quite large amount of hydrogen that can assist in defect passivation. In addition, the lower temperature and cost (compared to physical vapor deposition technique) make PECVD SiN even more attractive for photovoltaic industry. A systematic study of refractive index and hydrogen content for different deposition conditions was performed. Preliminary results of PECVD SiN deposition on crystalline and polycrystalline silicon cells are also presented in chapter 3. In chapter 4, an optimized process sequence for poly-Si solar cells is summarized. This process resulted in polycrystalline silicon cell with efficiency as high as 17.7%. Finally

chapter 5 describes the fabrication of single crystalline and polycrystalline silicon cells for optical processing to be done at NREL.

2. EFFECTS OF ILLUMINATION LEVEL ON DIFFUSION LENGTH AND EFFICIENCY OF POLY-Si CELLS

2.1 INTRODUCTION

Minority carrier lifetime is the most critical parameter indictating the performance of silicon solar cells. Several investigators have shown that the minority carrier diffusion length measured with the white light bias is generally higher in polycrystalline silicon cells than with no light bias. Ho et al. [1] found that the short circuit current, cell efficiency and diffusion length increased monotonically with the illumination level between 0 and 5 suns in polycrystalline EFG cells while the counterpart single crystal CZ cells did not show any increase in diffusion length. The increase in diffusion length was attributed to saturation or partial filling of distributed donor like state in p-type EFG material due to the movement of quasi fermi level. Structural imperfections (twins, dislocations, grain boundaries, etc.) and metallic impurities are the potential source of such distributed states in polycrystalline materials. Average short circuit current when plotted as a function of light intensity showed a slope of greater than unity (superlinearity) for EFG cells whereas single crystal cells maintained a slope of unity [1]. In addition, the superlinearity was found to be greater for lower performance EFG cells, suggesting that increased illumination level may shrink the gap between good and poor quality polycrystalline cells as well as between the polycrystalline and single crystal cells. The above results suggest the need and merit of investigating the degree of the enhanced diffusion length and performance of polycrystalline cells under concentrated light.

The objective of the section is four-fold: (a) quantify the illumination-induced increase in diffusion length using an analytical grain boundary model; (b) show that the diffusion length is not uniform but is a function of depth in illuminated polycrystalline materials; (c) determine the light induced diffusion length enhancement as a function of grain size, illumination level, and trap density; (d) perform solar model calculations, using the depth dependent diffusion length input into the PC-1D model [2], to estimate the impact of illumination level on polycrystalline cells ranging from thin film to large grain bulk poly.

2.2 THE GRAIN BOUNDARY MODEL

Polysilicon is a composite of crystallites joined at the grain boundaries. The grain boundary (GB) represents the transition between neighboring grains and consists of a large number of defects due to the incomplete atomic bonding. These defects are capable of trapping carriers and immobilizing them [3,4]. The lower chemical potential coupled with high density of states in the GB region accommodates the majority carriers which fill the trap states and act as recombination and scattering centers for minority carriers. In p-type polysilicon, grain boundary states are generally donor type. Therefore, unoccupied states above the fermi level in p-type material are positively charged, and induce a space charge region in the neighboring grains. Under optical illumination, a new occupancy of the trap states is established, and the equilibrium Fermi function is replaced by the quasi-Fermi function. Minority carriers generated by illumination are attracted to the charged trap states, thereby reducing the GB charge or potential from its dark value. To calculate the GB potential, a knowledge of the trap levels and their density is needed. Due to the lack of availability of a user friendly numerical model for polycrystalline materials, an analytical

model was used which assumes cubical grains and mono-energetic trap level for grain boundary states. This is consistent with the work of other investigators, [5-10]. It has been shown [4,5,8] that the dominant grain boundary states are located at E_i-E_t = 0.17 eV for p-type and E_t-E_i = 0.066 eV for n-type polysilicon. To further simplify the analysis, the following assumptions are used in our model calculations:

1. The material is composed of identical cubical grains of size D.
2. A discrete energy trap level exists at E_i-E_t = 0.17 eV fo the p-type materials analyzed in this study.
3. The depletion approximation is valid in the GB space charge region.
4. Impurity atoms are completely ionized and uniformly distributed.
5. Carriers trapped in the GB come from the GB space charge region of width W.

It is important to realize that even though we have used grain boundaries as dominant defects, dislocations can also be modeled by a similar barrier height model. Because of the number of assumptions (stated above) made to quantify this difficult problem, there could be some inaccuracies in the absolute values of diffusion length and cell efficiency. However, the calculated trends in the illumination enhanced effects on various polycrystalline materials should be reasonably accurate.

The effect of grain boundary states on mobility and lifetime are taken into account in our model. Details of this grain boundary model are published elsewhere [11,13], only the key equations pertinent to calculating the light-induced effects are briefly summarized here. By solving Poisson's equation and applying the charge neutrality condition to the GB and its

space charge region, the dark GB barrier height V_{go} can be expressed as [11]

$$V_{go} = \frac{qN_{ts}^2}{8\epsilon N} f_o^2(E_t, E_f) \tag{1}$$

where N_{ts} is the trap state density per cm^2, N is the doping density, and E_f is the Fermi-level at the GB. The Fermi function f_o is given by [16]

$$f_o = \frac{1}{1 + \frac{n_i}{N} e^{(qV_{go} + E_t - E_i)/kT}} \tag{2}$$

n_i and E_i represent the intrinsic carrier density and intrinsic Fermi level at the GB, respectively. Substituting (2) into (1), one obtains [13]

$$V_{go} = \left(\frac{q N_{ts}^2}{8\epsilon N}\right)\left[\frac{1}{1 + \frac{n_i}{N} e^{(q V_{go} + E_t - E_i)/kT}}\right]^2 \tag{3}$$

Equations (2) and (3) allow one to calculate the Fermi function and the GB barrier height in the equilibrium state. It can be seen that the trap density N_{ts} plays an important role in dictating the barrier height and the Fermi function. Equation (3) pertains to n-type material. Replacing f_o by $(1-f_o)$ and (E_t-E_i) by (E_i-E_t), Eq. (3) can be used for p-type material.

Under optical illumination, the equilibrium Fermi function is replaced by a quasi-Fermi function, and a new steady state is reached, which results in a reduction of V_g from its dark value.

In order to quantitatively study the reduction of V_g under illumination, relations between V_g and V_{go}, and effects of illumination level, trap density, and grain size were studied. By considering the dynamic balance between capture and emission of carriers at the GB trap states, one obtains [13]

$$V_g = V_{go}\,\beta^2 \tag{4}$$

$$G = \sigma\, V_{th}\left(\frac{6N_{ts}}{D}\right)\left[N e^{-qV_{go}\beta^2/kT}(1 - \beta f_o) - P_1 \beta f_o\right] \tag{5}$$

$$P_1 = n_i\, e^{(E_i - E_t)/kT} \tag{6}$$

where G is the photogeneration rate, D is the grain size, σ and V_{th} are the capture cross-section and thermal velocity for majority carriers, and $\beta = f/f_o$, the ratio of the quasi and dark Fermi functions in the dark.

V_{go} and f_o can be determined from Eq. (2) and (3). If G is known, β can be found from Eq. (5), and then the quasi-Fermi function and the grain boundary potential can also be determined. The dependence of the GB potential on the photogeneration rate and trap density can be deduced from Eq. (5). Since G is a function of depth under illumination, this relation was also utilized in our investigation of the depth variation. The photogeneration rate G is defined by the following integral over energy:

$$G(x) = \int N_{ph}(E)\ \alpha(E) e^{-\alpha(E)x}\, dE \tag{7}$$

where N_{ph} is the incident photon density, α the absorption coefficient, and x the depth from the surface. The dependence of G on x is discussed in the references [12,13,14].

Minority carrier mobility μ, lifetime τ, and diffusion length L are all function of V_g [13]. It is difficult to calculate the minority carrier mobility directly. Such is not the case, however, for the majority carrier. And there is also experimental evidence that the ratio of these two mobilities is nearly constant in both single- and poly-crystal silicon [15]. Thus, the minority carrier mobility μ may be expressed as

$$\mu = r\,\mu_{eff} \tag{8}$$

where r is about 2.5[15], and μ_{eff} is effective mobility. For doped materials, μ_{eff} is very close to the majority carrier mobility in polysilicon and can be represented by [13]

$$\mu_{eff} = \frac{1}{\frac{NkT}{A^*T^2D}e^{(V_g+\delta)/kT} + \frac{1}{\mu_s}} \tag{9}$$

where A* is the effective Richardson constant, μ_s the mobility in the grain, and $\delta = kT\ln(N_v/N)$. Above equation is generally more appropriate for the small grain materials where the carriers cross several grain boundaries. However, it tends to under estimate the mobility in large columnar grain polysilicon, especially with higher N_{ts}.

The electron lifetime τ_g associated with grain boundary recombination can be written as [13]

$$\tau_g = \frac{D}{3\gamma\, V_{th}\, \sigma_n\, N_{ts}} e^{-qV_g/kT} \tag{10}$$

The effective minority carrier lifetime can be expressed as

$$\frac{1}{\tau} = \frac{1}{\tau_g} + \frac{1}{\tau_s} \tag{11}$$

where γ is a constant (for high illumination $\gamma = 1/6$, for low illumination $\gamma = 1$), and τ_s is the lifetime in the grain.

In those cases where grain boundaries dominate the net recombination, τ_g is much smaller than τ_s, and τ is dominated by τ_g. In our calculations τ_s was assumed to be 164μs which is indicative of good intragrain quality and ensures that τ_g dominates the recombination.

Diffusion length can then be expressed as a function of V_g (or depth) by combining Eqs. (8-10), yielding

$$L = \left[\frac{kT}{q}\left(\frac{D}{3\gamma V_{th}\,\sigma_n\,N_{ts}}e^{-qV_g/kT}\right)\left(\frac{r}{\frac{NkT}{A^*T^2D}e^{(V_g+\delta)/kT} + \frac{1}{\mu_s}}\right)\right]^{1/2} \tag{12}$$

2.3 SOLAR CELL MODELLING

Solar cell efficiency calculations were performed using the PC-1D model [2] in a mode which allows external input file for bulk lifetime. A lifetime file was created for each cell with lifetime as a function of depth. Diffusion length or lifetime as a function of depth in the base was obtained from the grain boundary model. The lifetime profile was then fed into the PC-1D model, using the following n+pp+ cell configuration, to perform the numerical simulations.

1. Cell area of $1cm^2$
2. Series resistance of 0.02 ohm.
3. Erfc emitter doping, with $R_s = 100$ ohm/square.
4. P-type base with uniform doping of $1.0x10^{16}cm^{-3}$.
5. Cell thickness of 100 microns.
6. Erfc doping with surface concentration of $1 \times 10^{18}cm^{-2}$ in 0.5 μm thick BSF.
7. 4% shadow and reflective loss.
8. 98% effective back surface reflector.
9. FSRV of 500 cm/sec.
10. BSRV of $1.0x10^6$cm/sec.
11. Flat front and back surface.

2.4 RESULTS AND DISCUSSION

Fig. 1 shows the dependence of the GB barrier height on generation rate G. It can be seen that in the high G region, ($G > 10^{18}cm^{-3}s^{-1}$), V_g is modified by the illumination significantly, whereas in the low G region, ($G < 5x10^{17}cm^{-3}s^{-1}$), the change in V_g is very small, and the value of V_g is close to its dark value.

It should also be noticed that there is a flat band region where V_g approaches zero for the case of large grain size and high illumination. It was found that the larger grain size, higher concentration level, and lower trap density result in longer flat band region [13].

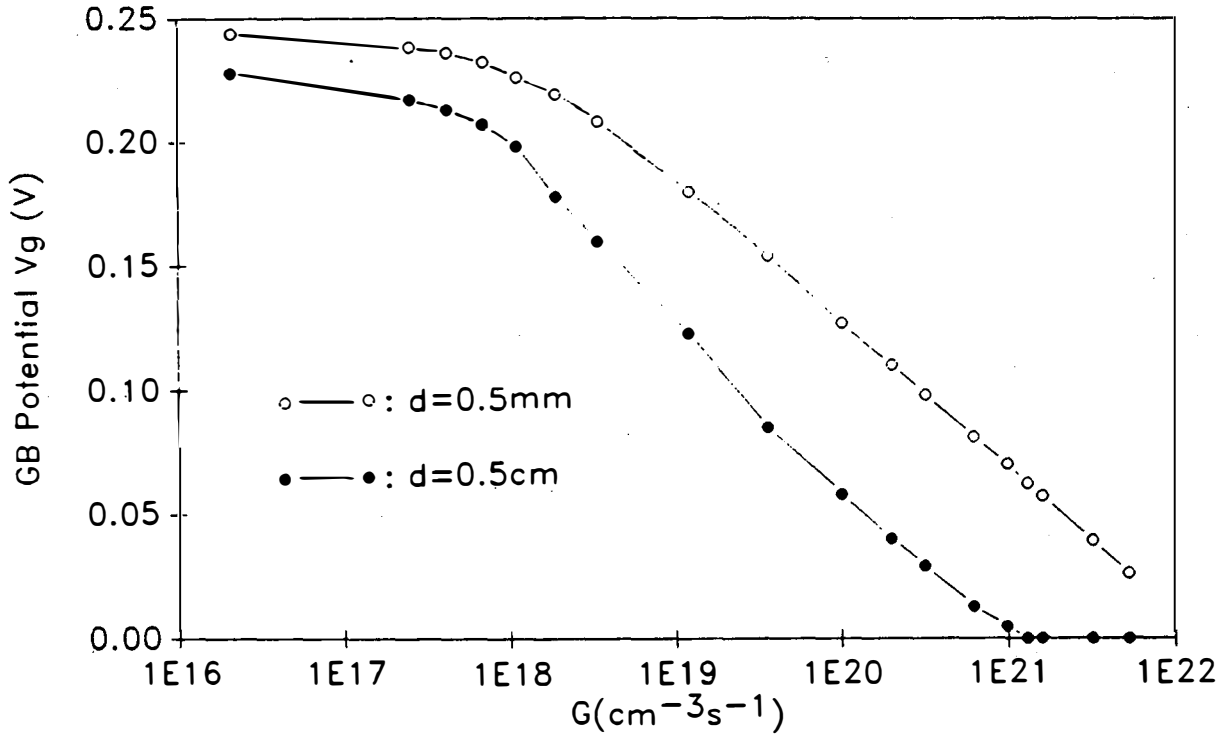

Fig.1 V_g as a function of generation rate for p-type poly-Si at Na=1E16(cm^{-3}), Nts=5E12(cm^{-2}).

Fig. 2 demonstrates the variation in diffusion length L at different concentration levels for two very different grain size (30 μm and 1 mm) materials with $N_{ts}=5x10^{11}$ cm^{-2}. It can be

seen that larger grain size and higher concentration level both improve the diffusion length significantly. The region in which L is constant, Fig. 2, corresponds to the flat band region where V_g equals zero.

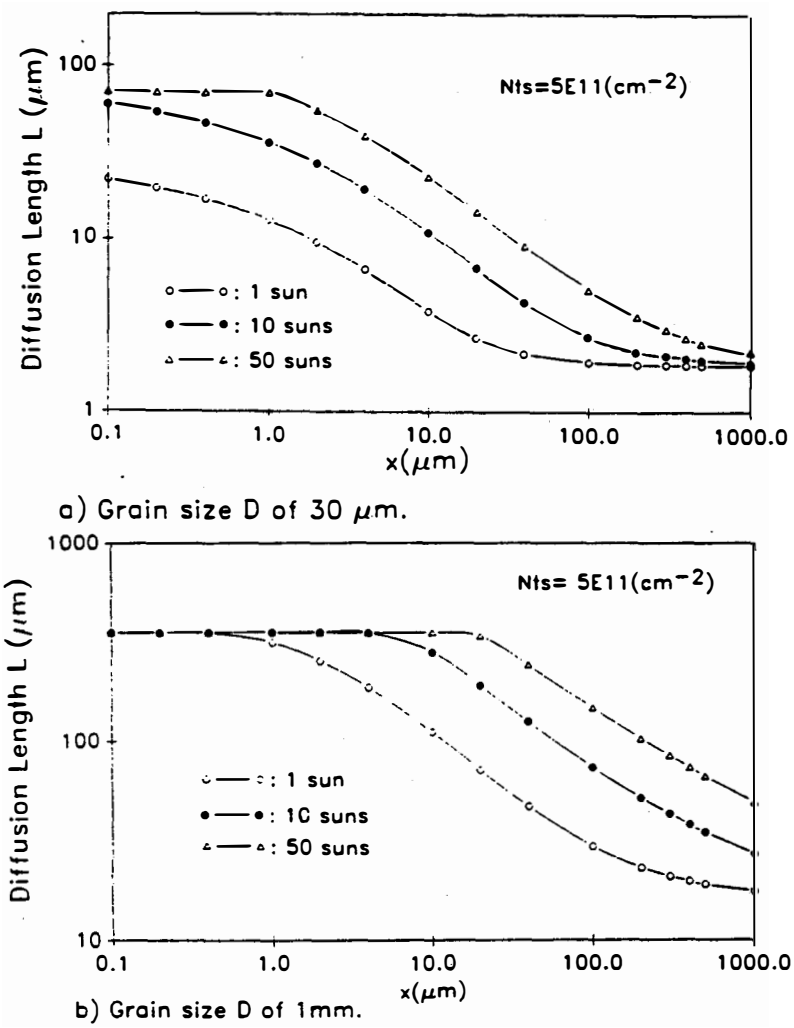

Fig.2 Concentration level effect on L for different grain size D

The results also indicate that a combination of higher concentration level, larger grain size and reduced thickness can significantly improve the average diffusion length of those poly-Si

materials in which grain boundary recombination is dominant. Fig. 2b shows that in a 1 mm grain size bulk poly with somewhat passivated grain boundaries ($N_{ts}=5x10^{11}cm^{-2}$), diffusion lengths as high as 350 μm are possible in the first 20 μm region at 50 suns. However, at one sun, diffusion length drops rapidly from 350 μm to less than 100 μm in the first 10 μm region.

In order to quantify the improvement in L due to concentration level for different D and N_{ts}, an improvement factor $\delta = L(50)/L(1)$ was defined, which is the ratio of L at 50 suns to that at 1 sun. Fig. 3 gives the variation of δ with N_{ts} and D at a depth of 10 μm. It is seen that the ratio increases rapidly with N_{ts} for small grain size ($D<30\mu m$), whereas, for large grain size (D=1mm), the ratio is close to one for N_{ts} less than $10^{12}cm^{-2}$.

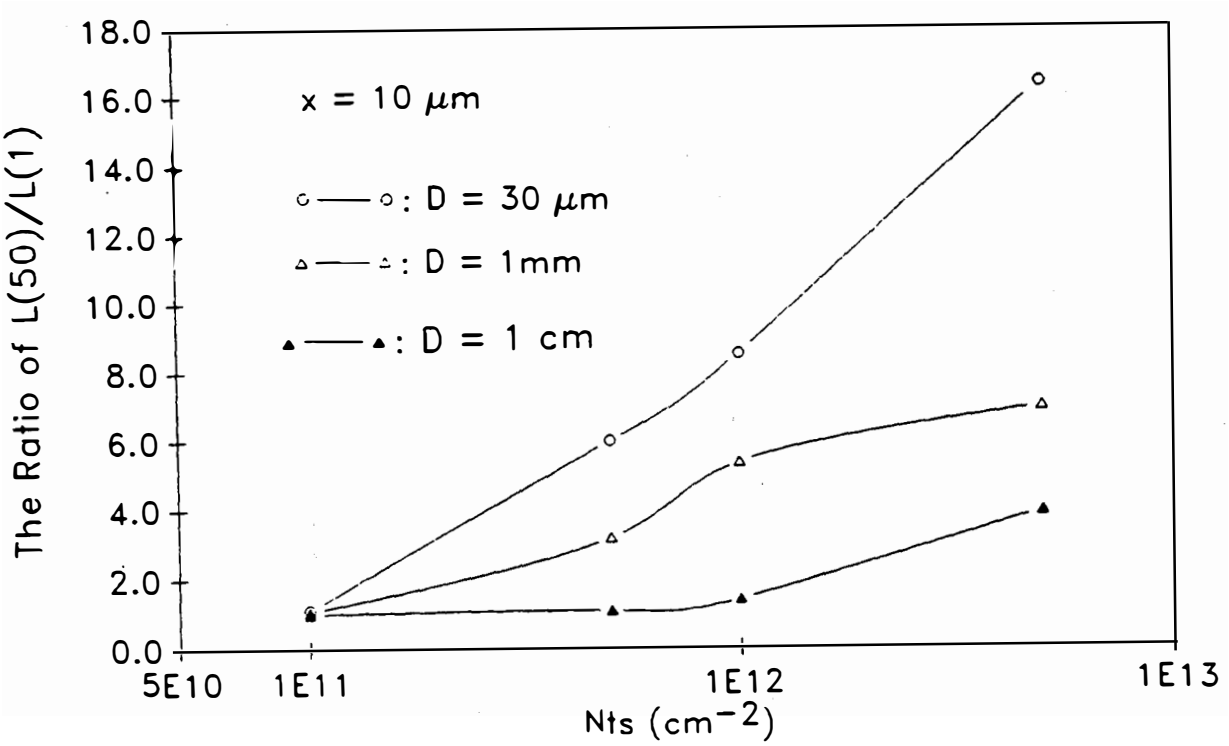

Fig.3 The effects of Nts and D on the ratio of L(50)/L(1).

Fig. 4 shows the effect of N_{ts} on depth dependence of δ for D of 30 μm. It indicates that the improvement in L due to illumination decreases with decreasing N_{ts}, and there is very little improvement in L for N_{ts} of $10^{11}cm^{-2}$ at which the ratio δ is one. The peaks in Fig. 4 are caused by the longer flat band region at 50 suns compared to one sun. It is interesting to note from Fig. 3 that $\delta \approx 1$ at N_{ts} of $10^{11}cm^{-2}$ regardless of the grain size D and the material behaves very much like single crystal where there is no light-induced enhancement in L.

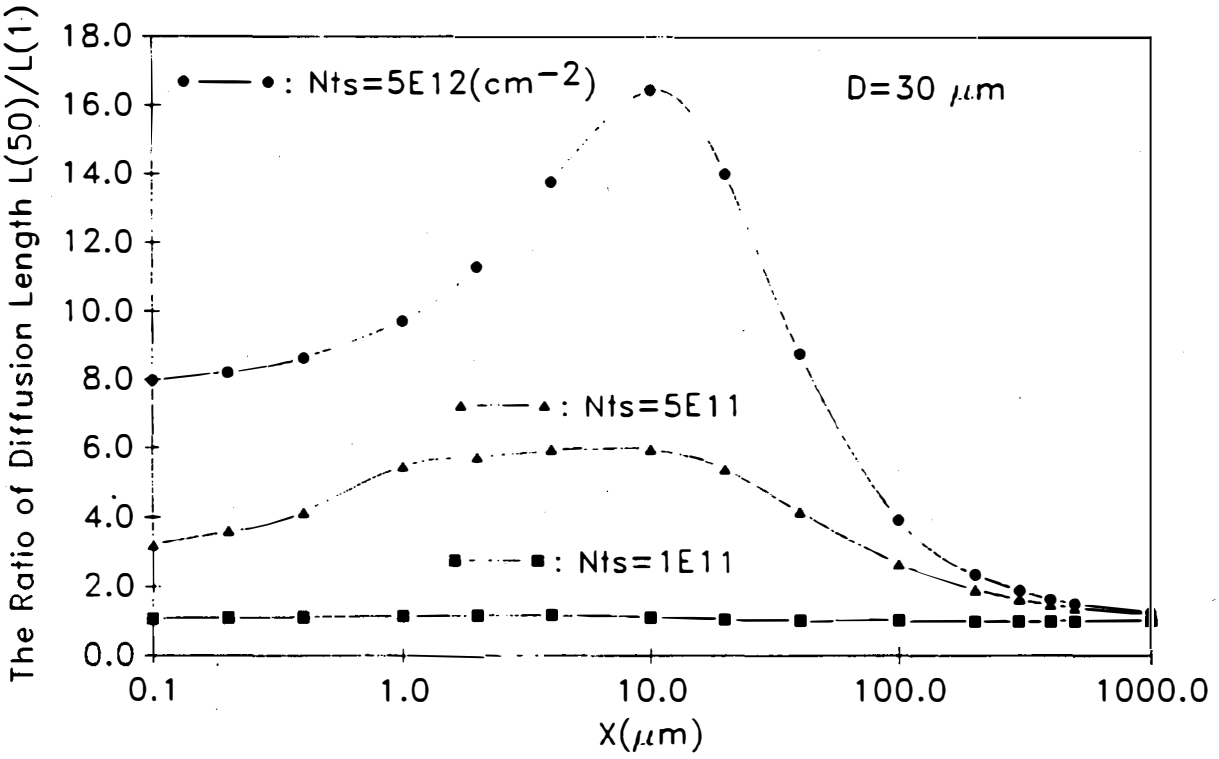

Fig.4 Trap density Nts effect on the ratio of diffusion length.

It is important to recognize that the illumination level enhanced diffusion length in polysilicon adds to the normal increase in cell efficiency due to concentrated sunlight. Cell efficiency calculations in Fig. 5 show that a single crystal cell with L=318μm and a 1 mm grain size polysilicon cell with $N_{ts} = 10^{11}cm^{-2}$ and L=318 μm respond exactly the same way to the concentrated light. Both the cells start with one sun efficiency 14.9% and end up with an efficiency of 17.2% at 50 suns. However, as N_{ts} increases to $10^{12}cm^{-2}$, polycrystalline diffusion length drops and one sun efficiency falls to 11.87%, but the efficiency at 50 suns remains ~17% due to greater diffusion length enhancement in polysilicon with higher N_{ts}. Thus, the undesirable effects of grain boundary states in the density range of 10^{11}-$10^{12}cm^{-2}$ are nearly eliminated under 50 suns for this large grain polysilicon. As the trap density increases to $5x10^{12}cm^{-2}$ a bigger relative improvement in efficiency (η_{50}/η_1) is observed but the absolute efficiency (14.4%) falls short of 17% at 50 suns. It is important to realize that N_{ts} can be different for the same grain size material because of different degree of grain boundary passivation or due to the difference in the impurity content and nature of the grain boundaries. These calculations show that increased illumination level can reduce the gap between good and bad polysilicon. Fig. 5 shows that the majority of the efficiency improvement due to this effect can be realized with a illumination level of ~30 suns. It is important to recognize that even in a columnar large grain polysilicon, the diffusion length in the interior of the grain becomes a function of depth for τ_s = 164μs because of the two effects. First, V_g or recombination velocity along the grain boundaries increases as a function of depth under the illumination and secondly, grain boundary recombiantion velocity at any depth affects the recombination in the interior of the grain laterally upto a distance of 2 to 3 diffusion lengths from each boundary.

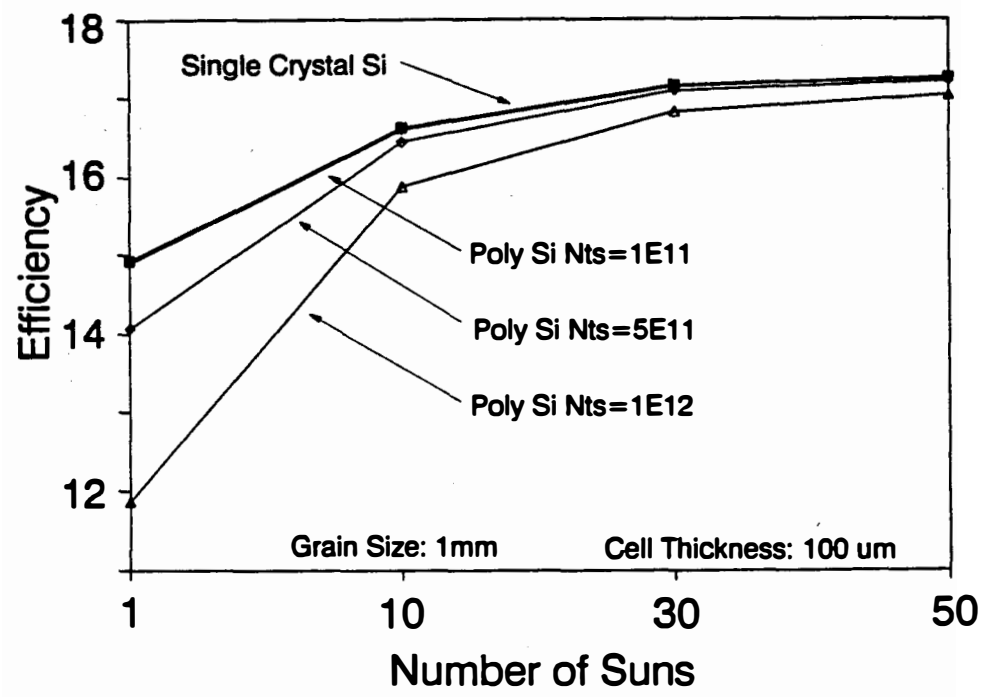

Fig. 5 The effect of concentration level and trap density on the efficiency.

Fig. 6 shows that the relative improvement in efficiency (η_{50}/η_1) is much greater for polysilicon with smaller grain size and higher N_{ts}. Model calculations show that, a 30 μm grain size cell with $N_{ts} = 5x10^{11}$ cm^{-2} has one-sun efficiency of only 3.9% which increases to 11.6% at 50 suns primarily due to the enhanced diffusion length effect. Further calculations indicate that this efficiency can be increased to 13.4% by reducing the polysilicon thickness

from 100 μm to 40 μm. This is the result of higher average diffusion length in thin film poly. Thus, increased illumination level does not completely eliminate but certainly mitigates the undesirable effects of small grain size and high defect density at the grain boundaries.

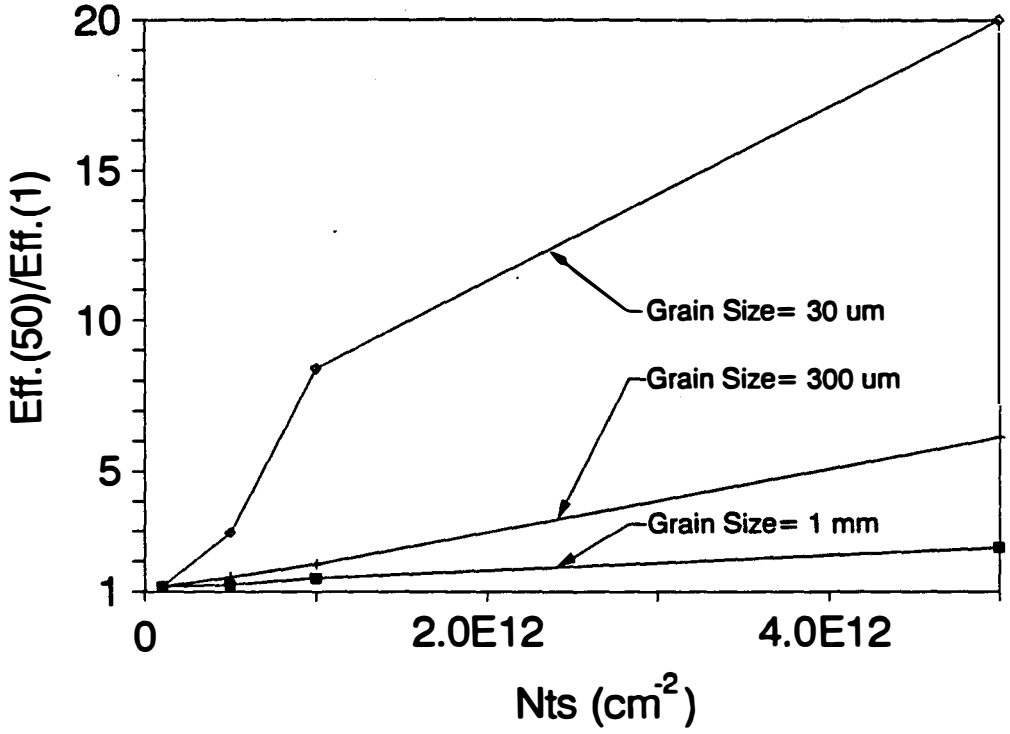

Fig. 6 The effect of trap density and grain size on the efficiency

2.5 CONCLUSIONS

A combination of grain boundary model and solar cell modelling is used to quantify the effect of illumination level on diffusion length and efficiency of polysilicon cells. It was found that diffusion length is not uniform under illumination for those polysilicon materials in which grain boundaries dominate the recombination. The grain boundary barrier height decreases and diffusion length increases as we approach the illuminated surface. The relative improvement in diffusion length and efficiency increases with the concentration level. The illumination level enhanced diffusion length boosts the normal increase in efficiency under concentrated sunlight. It is shown that in a large grain (1mm) polysilicon, an increased illumination level of 50 suns can eliminate the undesirable effects of a grain boundary state density in the range of 10^{11}-10^{12}cm^{-2}. The majority of the efficiency improvement due to enhanced diffusion length effect can be realized at ~30 suns.

Model calculations were also performed for small grain thin film polysilicon cells. It was found that the efficiency of a 30 μm grain size polysilicon cell, with $N_{ts}=5x10^{11}cm^{-2}$, can increase from 3.9% at one sun to 11.5% at 50 suns. Reducing the cell thickness to 40 μm from 100 μm, without any light trapping, raises this efficiency to 13.4% because of the increased average diffusion length. The illumination level induced diffusion length enhancement effect is more pronounced in polysilicon materials with smaller grain size and higher N_{ts}. Hence, the illumination enhanced diffusion length in polysilicon can reduce the efficiency gap between the cells made on: a) good and bad polysilicon; b) polysilicon with passivated and non-passivated grain boundaries; c) polysilicon with different grain size; and d) polysilicon and single crystal silicon.

3. Effects of Deposition Conditions on the Refractive Index and Hydrogen Content of PECVD Silicon Nitride Films

3.1. Introduction

Recent studies [17-19] show that the application of PECVD-SiN thin film can be very helpful in improving efficiency of silicon solar cells. It not only acts as an antireflection coating layer with a suitable refraction index, but can also serve as a source for hydrogen passivation to improve the performance of selected devices. This is because PECVD processing can produce quite large amount hydrogen atoms during deposition. The above two fold advantage makes PECVD-SiN film a very attractive material in solar cell fabrication.

SiN has been found to act as a means of passivating defects for both crystalline and polycrystalline silicon solar cells, in addition to its role as an AR coating material. The improvements in the minority carrier diffusion length and quantum efficiency due to PECVD SiN have been studied [17 - 19] and the beneficial effects of PECVD SiN on short circuit current , open circuit voltage, and cell efficiency have been reported [20 - 22]. However, there is a large variation in the reported SiN film deposition conditions and the correlation between all these improvements and PECVD deposition conditions is still not fully understood. In order to find the optimum deposition condition, a systematic study was conducted in the research.

The major concerns in usual SiN film for solar cell application are its refractive index and hydrogen concentration. In this report refractive index and hydrogen content for different deposition conditions was determined. Three major deposition parameters, deposition temperature, reactant ratio, and rf. power, were varied. The results show that

the refractive index strongly depends on the ratio of NH_3 and SiH_4. The effects of substrate temperature and rf. power on the refractive index and growth rate are also presented. Hydrogen concentration was monitored by FTIR. It is found that the concentration of Si-H bonds is very sensitive to substrate temperature, which in turn is proportional to the hydrogen content in the SiN films. A shift in the peak position of Si-H stretching mode was observed with the ratio of NH_3/SiH_4 , which is indicative of the change in the N/Si ratio in the films. The concentration of N-H and Si-N bonds were also monitored by FTIR. The effects of NH_3/SiH_4 ratio, substrate temperature and rf. power on the concentration and configuration of Si, N, and H are discussed. The results of refractive index and hydrogen content in this study should provide useful guidelines on process optimization of SiN films used for both antireflection and hydrogen passivation purposes.

3.2. Experiment

Plasma-enhanced silicon nitride thin films (PECVD SiN) were prepared in series 700 Plasma-Therm Inc reactor operated at 13.6 KHz. The gases used were SiH_4, NH_3 and N_2, total pressure was 0.9 Torr, temperature was varied in the range of 150 to 350 °C, and the rf power was varied in the range of 20 - 100 W.

Silicon nitride films were characterized by FTIR spectrometer (BIO-RAD,3240-spc system) to study hydrogen concentration and chemical bonding configurations between Si, N, and H in the films. SiN films were deposited on high resistivity (> 200 ohm-cm) FZ (100) Si substrates that were polished on both sides to reduce infrared transmission loss. A four wave-number resolution was chosen, and sixty four scans were averaged for each spectrum. The refractive index and thickness of SiN films were measured by Ellipsometer (Thin film measurement system, SD 2300, PlasMos) at 632.8 nm wavelength.

The sample ID, deposition conditions, and correspondent thickness are listed in Table 1.

3.3. Substrate temperature effects

a. Hydrogen content study by FTIR

Variation of hydrogen concentration in SiN films deposited at different substrate temperature was monitored by absorption infrared spectrum. The infrared spectrum contains three major peaks of interest: a strong absorption peak at 820 cm^{-1} due to a Si-N vibration; another absorption peak at 2170 cm^{-1} due to Si-H vibration; and a weak absorption peak at 3350 cm^{-1} due to N-H vibration.

A typical infrared spectrum of SiN on Si substrate obtained in our experiment is shown in Fig.1, in which the relevant peak positions are indicated. The peak at 610 cm^{-1} is due to a two phonon Si lattice absorption. Deposition temperature effects on infrared spectrum are shown in Figure 2 in which the spectrum labelled as HRSIO is for silicon substrate only with no SiN film; while spectrums HRSIN150, HRSIN200 and HRSIN300 are after the SiN film deposition at temperatures of 150, 200 and 300 °C, respectively.

Quantitative correlation between hydrogen content and the area under Si-H and N-H absorption peaks of infrared spectrum, calibrated by nuclear reaction measurements, has been made by Lanford etc.[23]. They pointed out that Si-H bonds have about 1.4 times the specific absorption of N-H bonds in SiN films and the hydrogen content can be determined by measuring normalized area under Si-H and N-H absorption peaks. We have not done that yet.

Significant changes in the Si-H and N-H peaks with the deposition temperature were

observed, Figure 2. The area under the Si-H and N-H absorption peaks increases with decreasing temperature. Another absorption peak in Figure 2, the shoulder around 1200 cm $^{-1}$, was also found to be temperature dependent. This shoulder is assigned to the N-H bending vibration in Si-NH-Si group [24]. It can be seen that this shoulder height is proportional to the absorption peaks of N-H and Si-H.

b. Refractive index and growth rate

The variation in refractive index n and growth rate R as a function of deposition temperature are shown in Figures 3 and 4, respectively. Figure 3 shows that refractive index can be adjusted in the rage of 1.9 to 2.2 by changing substrate temperature in the range of 150 and 350 °C. Film growth rate increases with substrate temperature as shown in Fig.4

3.4. Effects of NH_3/SiH_4 ratio

a. Effect on refractive index and growth rate

Refractive index was found to be a strong function of gas flow ratio NH_3/SiH_4. The experiment on the ratio was conducted in the range of 0 to 1.2. Figure 5 shows that refractive index decreases rapidly in the lower ratio regime and level off around the value of 2.0 in the higher ratio regime (NH_3/SiH_4 > 0.8). When the ratio is zero, the film is most likely an amorphous silicon film, even though N_2 is used in the process. With increasing the ratio until 0.75, the value of n can be controlled from 3.5 to 2.0, while n remains constant with further increase in the ratio. Figure 6 shows the ratio effect on the growth rate of the films. The result shows that growth rate increases slightly with the ratio.

b. Effect on infrared spectrum

The variation of NH_3/SiH_4 ratio on infrared spectrum is shown in Figure 7 in which spectrum HRSIO for silicon substrate only and HRSINH30, HRSINH315, and HRSINH345 spectrums for the NH_3/Si_3H_4 ratio values of 0, 0.375, and 1.125, respectively. Two interesting features are seen in Figure 7: (i) Si-H absorption peak position shifts to longer wave-number with the increasing ratio; (ii) for the ratio equal to zero, no N-H absorption peak is detected, and the N-H absorption intensity increases with the ratio. The shift of Si-H peak position provides useful information about the N/Si ratio in the films, which can be expressed as [25]:

$$\gamma\ (cm^{-1}) = 2018 + 193\ N/Si$$

where γ is the Si-H absorption peak position, and N/Si is the ratio of in the film.
It can also be seen from Fig.7 that the absorption intensities at 820 cm^{-1} and the shoulder around 1200 cm^{-1} all increase with NH_3/SiH_4 ratio. Figure 8 presents an enlarged view of Si-H and N-H absorption peaks as a function of the ratio of NH_3/SiH_4, which indicates the shift of Si-H peaks and changes in the area under N-H absorption peaks with NH_3/SiH_4 ratio more clearly.

3.5. Effects of varying rf power

a. Effects on growth rate and refractive index

rf power used during PECVD SiN deposition was controlled in the range of 30 to 100 W. The growth rate variation as a function of rf power is shown in Figure 9. An oscillating change in the growth rate was observed, which suggests the two competing processes, deposition and etching, exist during PECVD SiN processing. The growth rate varies from 90 to 120 A^o for the rf power in the range of 30 to 100 W. The refractive index n is also slightly changed with rf power. It can be controlled from 1.92 to 2.1 for the power

between 30 and 100 W. The variation of n with rf power is shown in Figure 10.

b. Effects on infrared spectrum

The changes in infrared spectrum of SiN films on silicon substrate with different rf power are shown in Figure 11, in which the spectrum HRSIO is for silicon substrate only, and spectrums HRSINH33, HRSINPRF50, HRSINPRF75, and HRSINPRF100 are for rf power 30, 50, 75, and 100 W, respectively. It was found that Si-H absorption is not very sensitive to rf power and N-H absorption increases slightly with the rf power. On the other hand, Si-N absorption is enhanced appreciably by increasing rf power.

3.6. Improvements in cell efficiency due to double layer SiO_2/SiN AR coating

Experiments were conducted to deposite double layer deposition of SiO_2/SiN AR coating on both crystalline and polycrystalline Si cells. The preliminary results are summarized in Table 2 and Table 3 for crystalline and polycrystalline Si cells, respectively. More than 50 % improvement in J_{sc} for both single- and poly- Si cells was obtained along with significant improvement in V_{oc} for single crystal Si cells and the improvement in FF for poly-Si cell. It should be noted that these results are only preliminary and further experiments are underway to fully understand mechanisms behind PECVD and annealing processes induced improvement in cell performance.

3.7. Conclusions

Systematic study of the effects of deposition temperature, reactant ratio and rf power on refraction index, growth rate, and Si-H, N-H, Si-N absorptions has been conducted. The results show that refractive index of SiN film can be adjusted by controlling substrate temperature, rf power, and gas flow ratio NH_3/SiH_4. Hydrogen contents in SiN films can be monitored by Si-H and N-H vibration modes in the FTIR absorption spectrum. FTIR

study indicated that hydrogen content in SiN films is strong function of deposition temperature, and it increases with decreasing of the temperature.

The results of refractive index and hydrogen concentration in this study should help in finding an optimum deposition condition for SiN film used for silicon solar cell application. Experiments are now in progress to deposit these films on solar cells. Solar cell performance is being monitored and analyzed to separate and quantify the AR coating and defect passivation effects of PECVD SiN films.

Table 1. Sample ID, deposition conditions and film thickness.

Sample	T(C°)	NH_3/SiH_4	P_{RF}(W)	t(A°)
HRSIO	0	0	0	0
HRSINH30	275	0	30	2914
HRSIN315	275	.375	30	2976
HRSINH33	275	.75	30	3254
HRSINH345	275	1.125	30	3317
HRSINPRF50	275	.75	50	3650
HRSINPRF75	275	.75	75	2770
HRSINPRF100	275	.75	100	3245
HRSIN150	150	.75	30	2140
HRSIN200	200	.75	30	2685
HRSIN300	300	.75	30	3043

ID#	I_{sc}(mA)	V_{oc}(V)	FF	Eff(%)	
11	22.02	.601	.7915	10.48	
A11	34.57	.653	.7797	17.61	
AA11	35.15	.649	.7859	17.93	
	59 %			71 %	Gain
12	22.18	.603	.7554	10.1	
A12	35.19	.651	.6747	15.46	
AA12	35.87	.650	.7533	17.57	
	62 %			73 %	Gain
21	22.13	.601	.7959	10.58	
A21	34.75	.650	.7941	17.94	
AA21	35.56	.655	.7949	18.53	
	60 %			75 %	Gain
31	22.02	.600	.8001	10.57	
A31	34.32	.637	.7903	17.27	
AA31	35.7	.654	.7843	18.32	
	62 %			73 %	Gain

Table 2. The improvements in crystalline Si cell performance due to SiO_2/SiN AR coating.
A = after AR coating, AA = AR + Annealing(350°C, 10 min.)

ID#	I_{sc}(mA)	V_{oc}(V)	FF	Eff(%)	
14	22.74	.566	.637	8.2	
AA14	35.34	.572	.717	14.52	
	55 %			77 %	Gain
23	23.4	.57	.637	8.51	
AA23	35.62	.576	.6778	13.9	
	52 %			63 %	Gain
24	22.7	.565	.613	7.87	
AA24	34.8	.571	.649	12.88	
	53 %			63 %	Gain
33	23.19	.569	.641	8.45	
AA33	35.33	.573	.674	13.65	
	52 %			61 %	Gain

Table 3. The improvements in poly-Si cell performance due to SiO_2/SiN coating.
AA = AR coating + Annealing (350°C, 10 min.).

Fig.1 A FTIR spectrum for SiN film on Si substrate.

Fig.2 Infrared spectrum of SiN films prepared at different deposition temperature. The samples ID and their deposition condition are listed in Table 1.

Fig.3 Refraction index as a function of substrate temperature.

Fig.4 The variation of growth rate with deposition temperature.

Fig.5 The variation of refraction index with NH_3/SiH_4 ratio.

Fig.6 Growth rate as a function of NH_3/SiH_4 ratio.

Fig.7 Infrared spectrum of SiN films prepared with different NH_3/SiH_4 ratio.

Fig.8 The effect of NH_3/SiH_4 on Si-H peak position and N-H absorption.

Fig.9 RF power effect on SiN film growth rate.

Fig.10 RF power effect on SiN film refraction index.

Fig.11 Infrared spectrum for different deposition rf power.

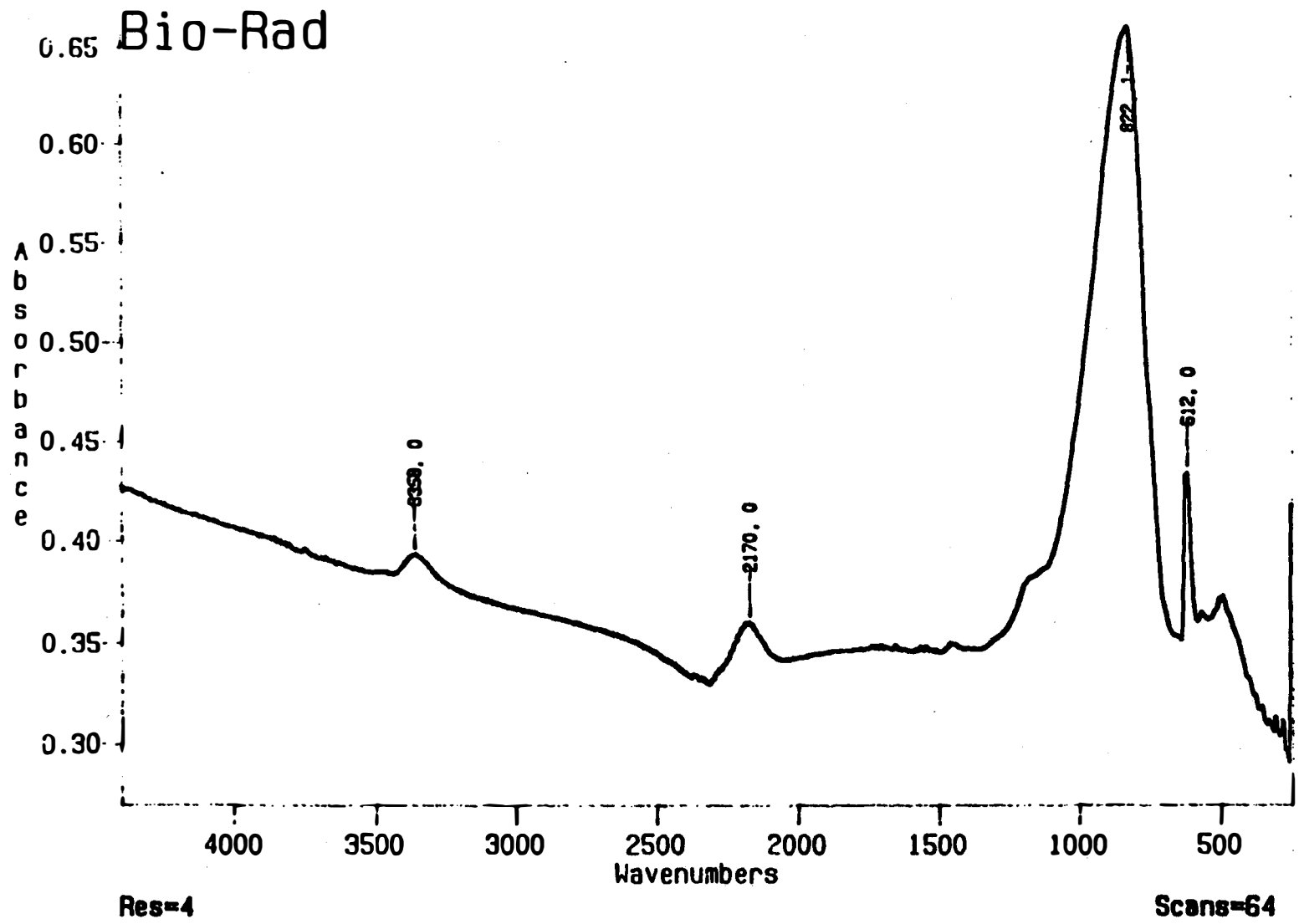

A FTIR spectrum for SiN film on Si substrate.

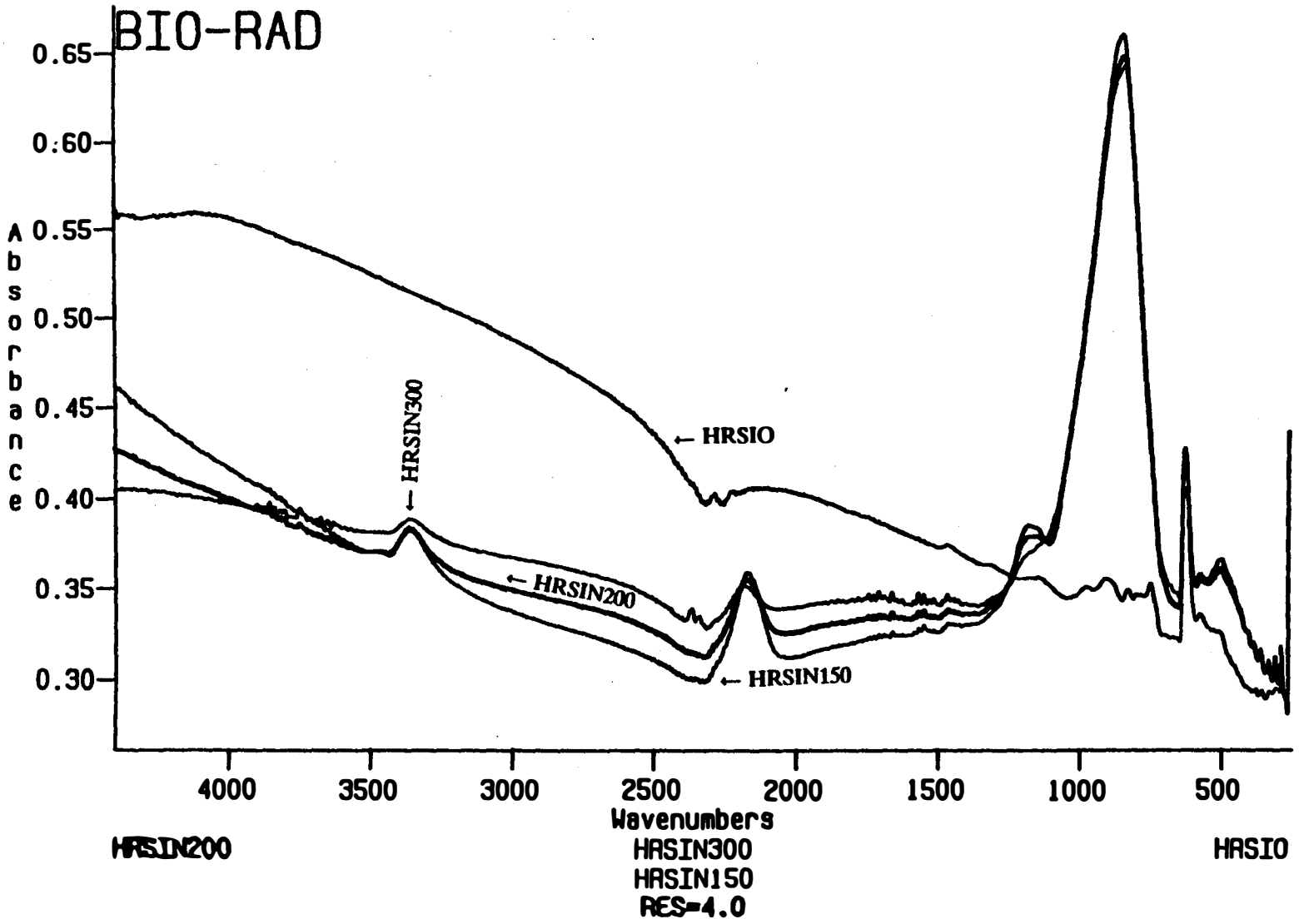

Fig.2 Infrared spectrum of SiN films prepared at different deposition temperature.

The samples ID and their deposition condition are listed in Table 1.

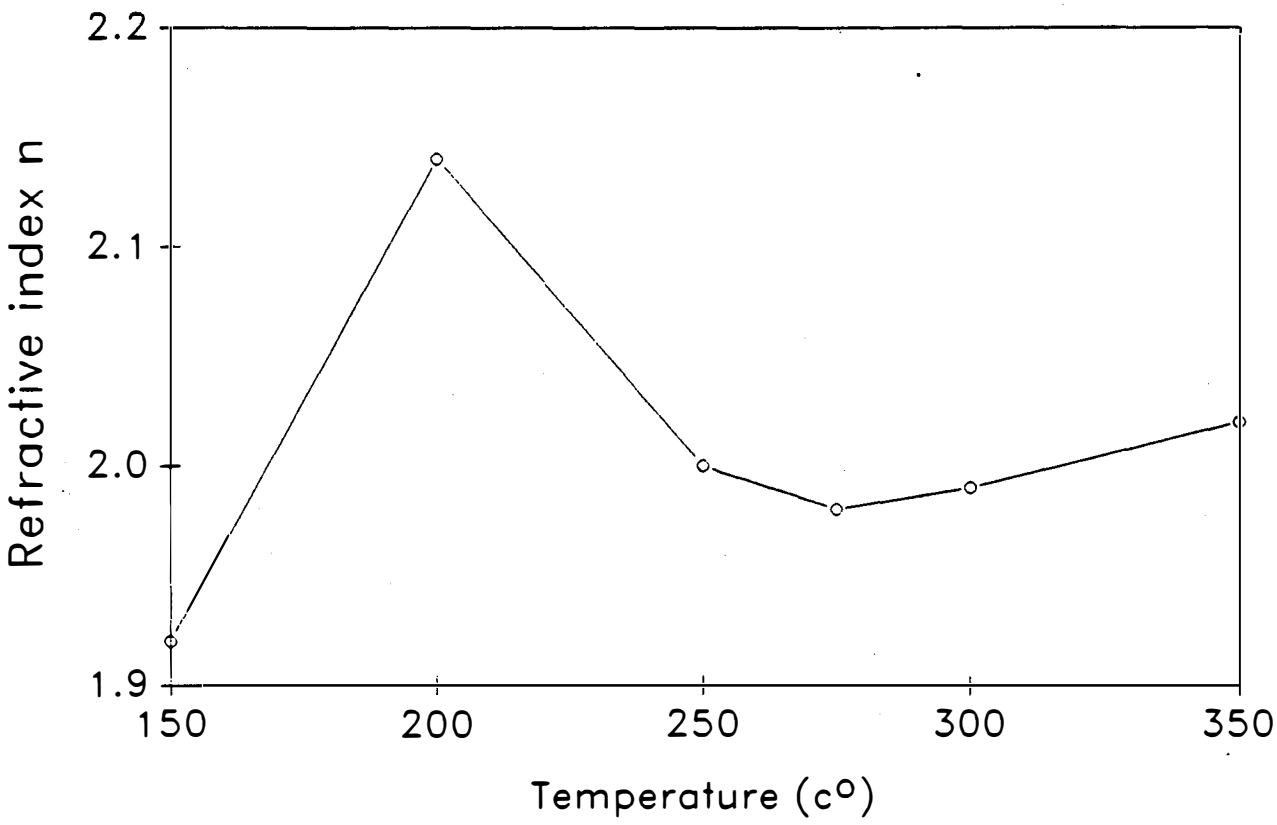

Fig.3 Refraction index as a function of substrate temperature.

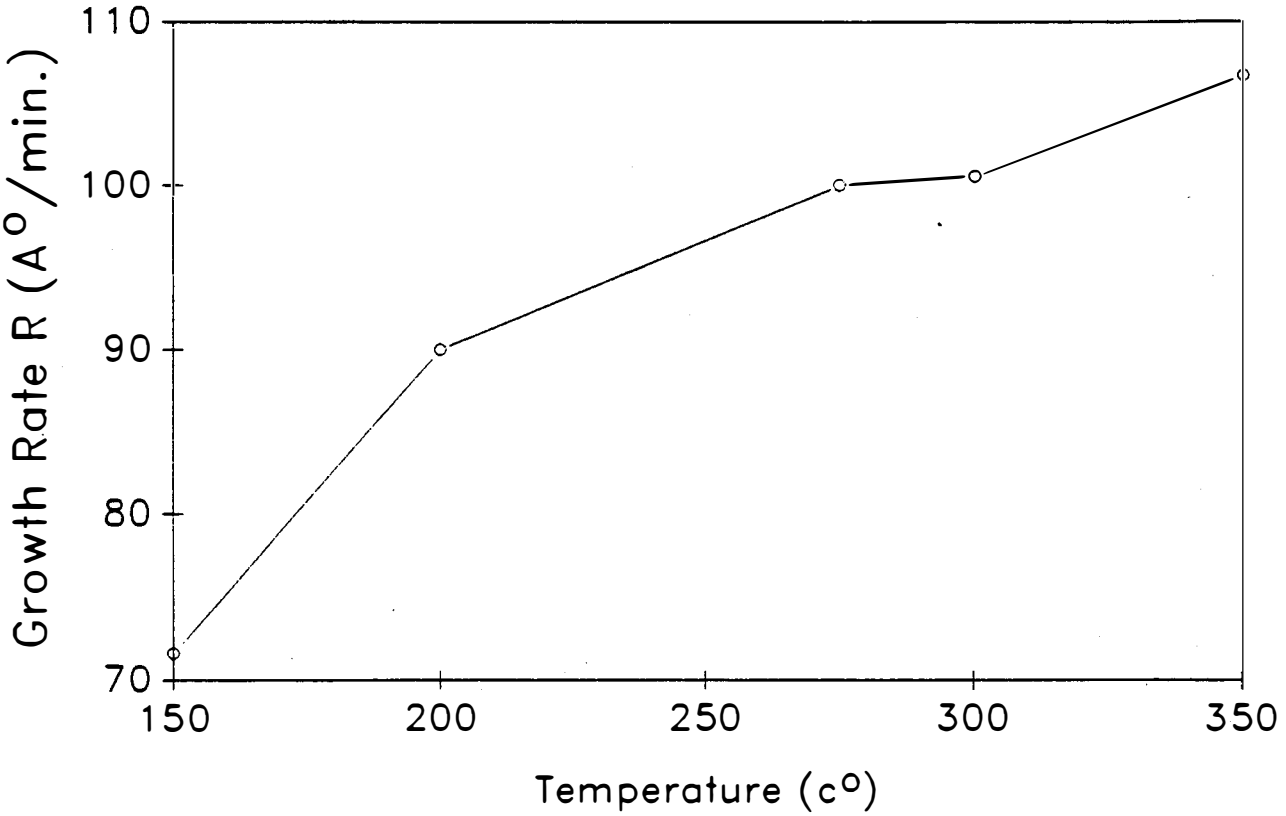

Fig.4 The variation of growth rate with deposition temperature

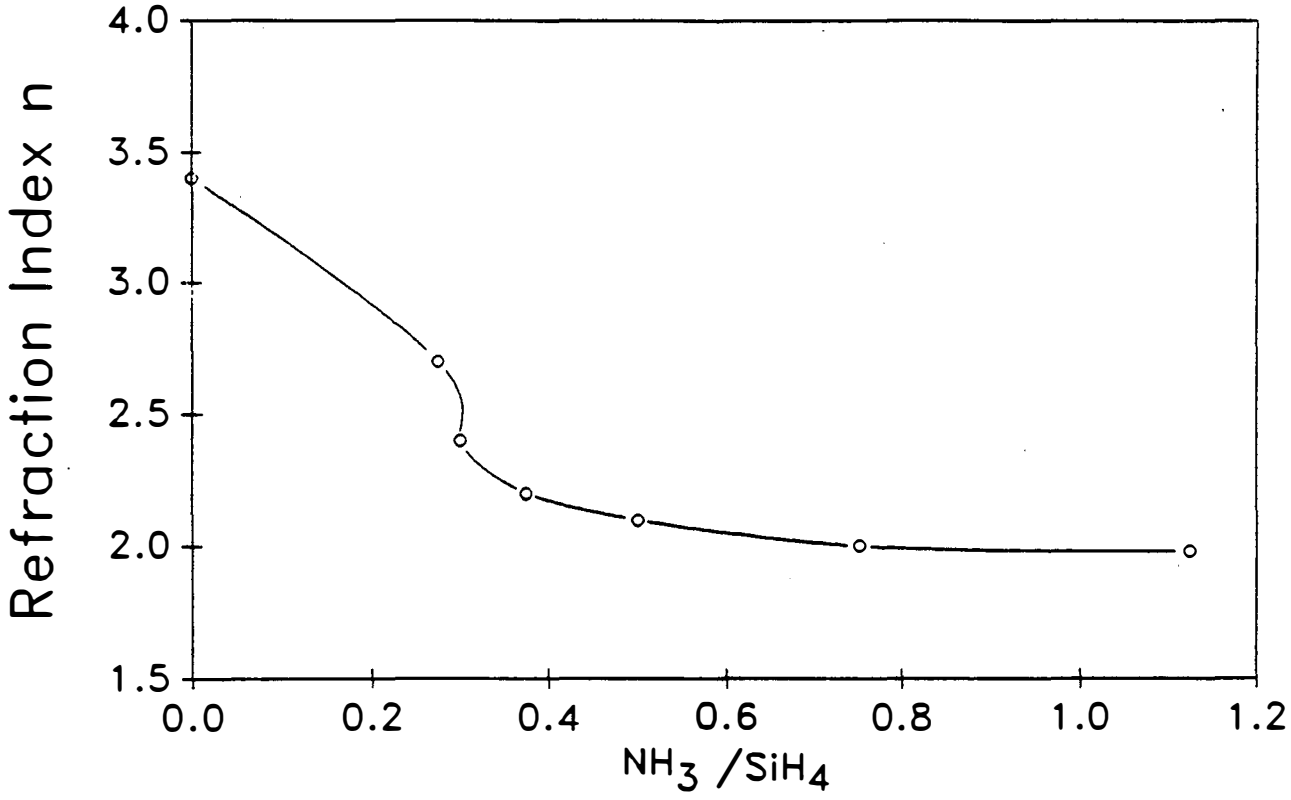

Fig.5 The variation of refraction index with NH_3/SiH_4 ratio.

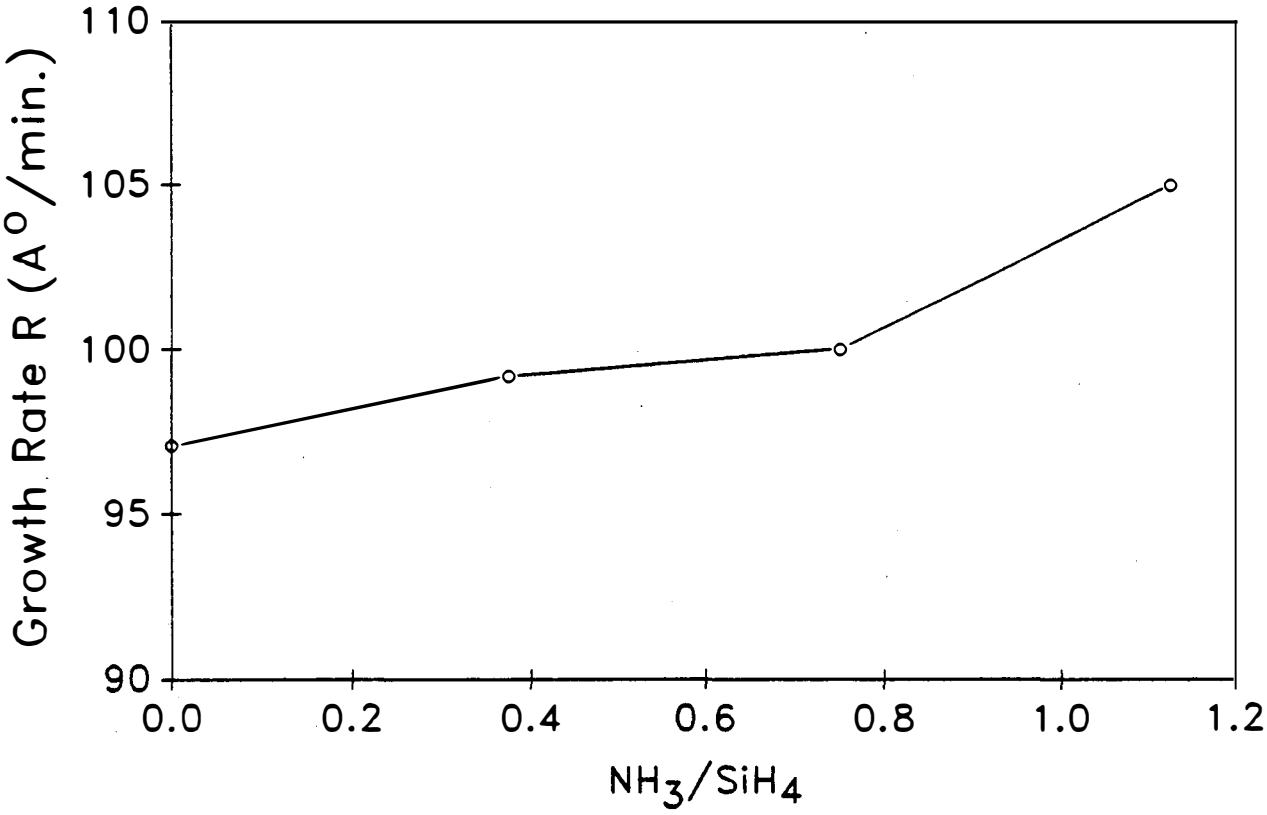

Fig.6 Growth rate as a function of NH_3/SiH_4 ratio.

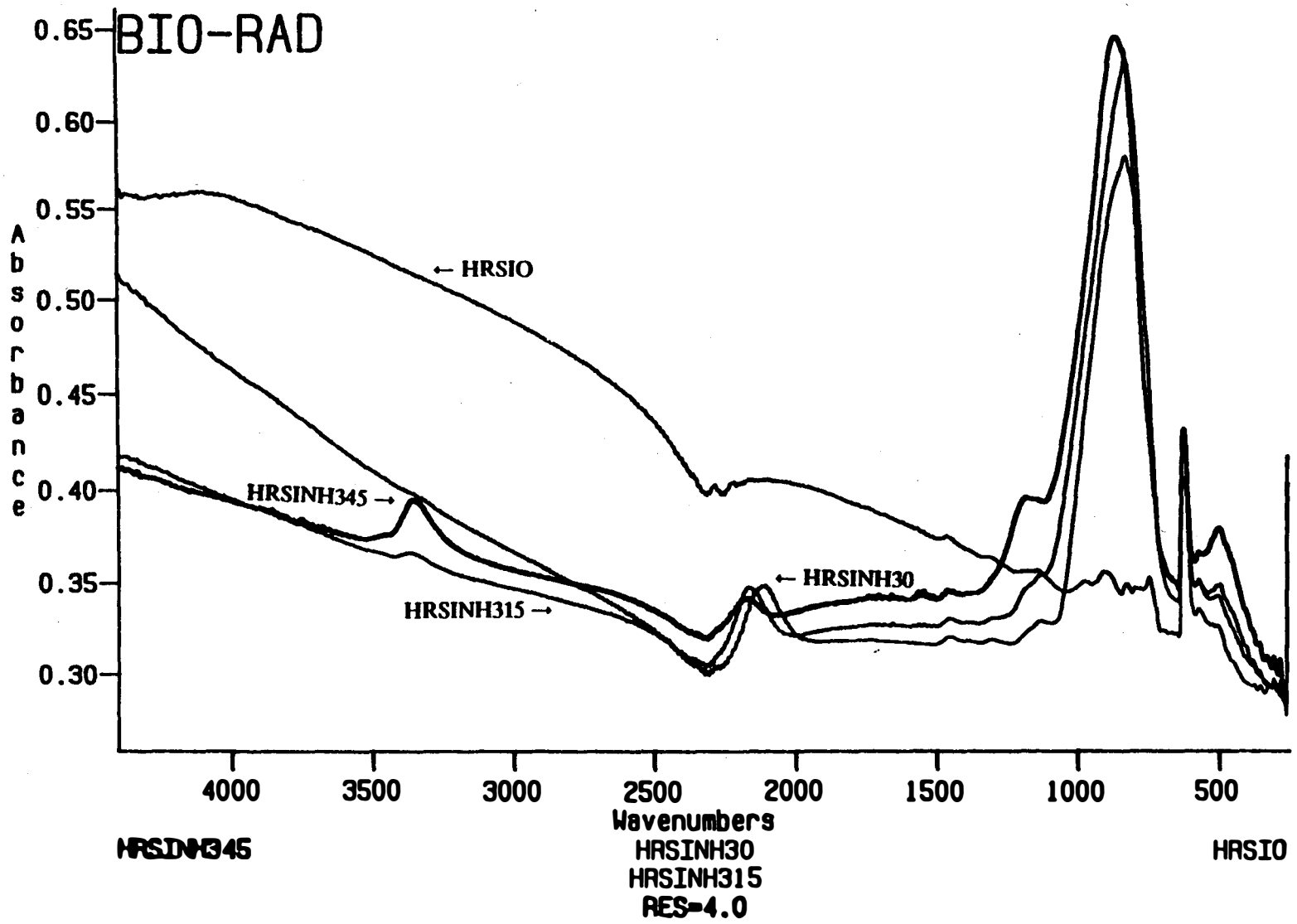

Fig.7 Infrared spectrum of SiN films prepared with different NH_3/SiH_4 ratio.

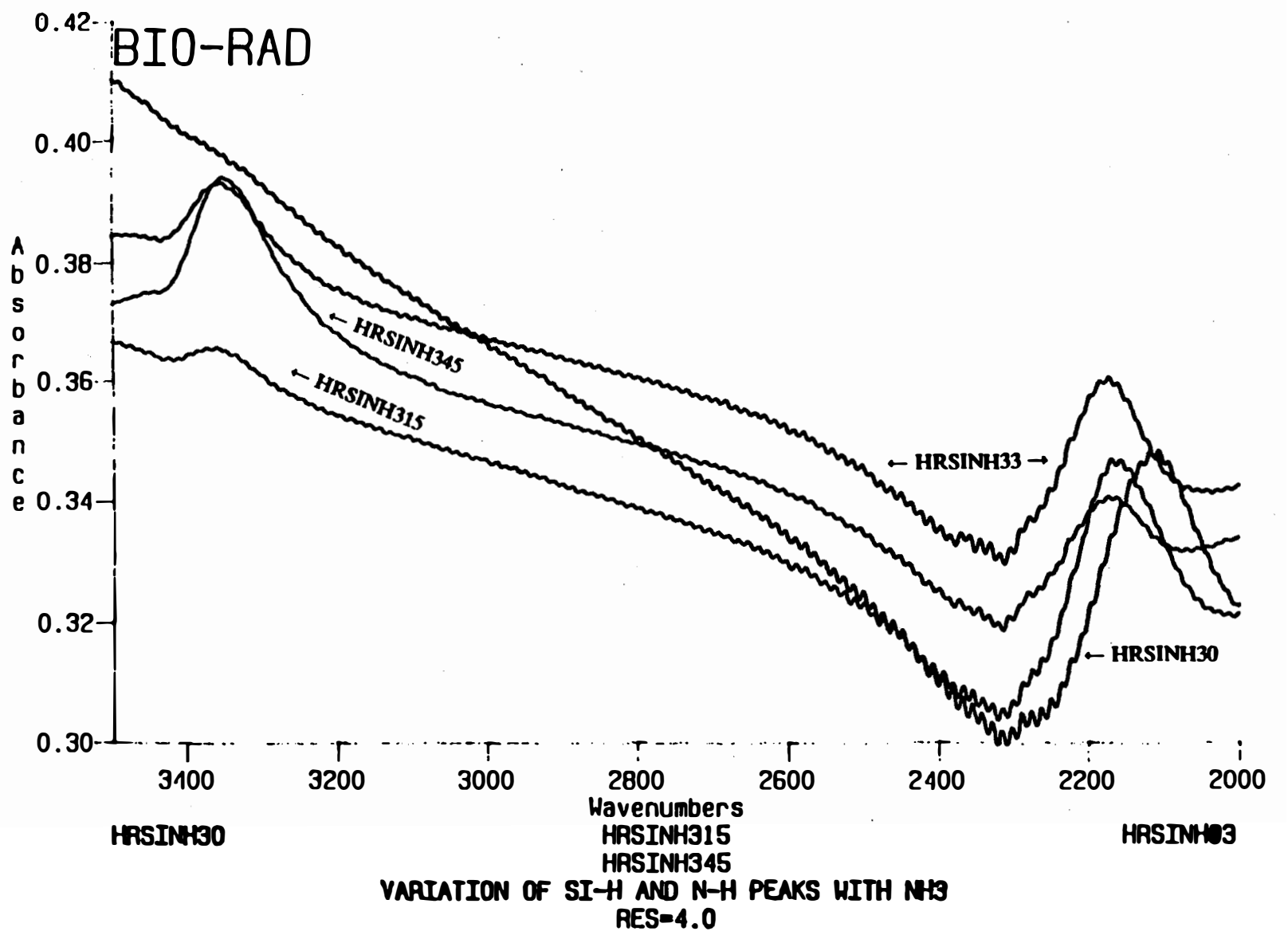

Fig.8 The effect of NH_3/SiH_4 on Si-H peak position and N-H absorption.

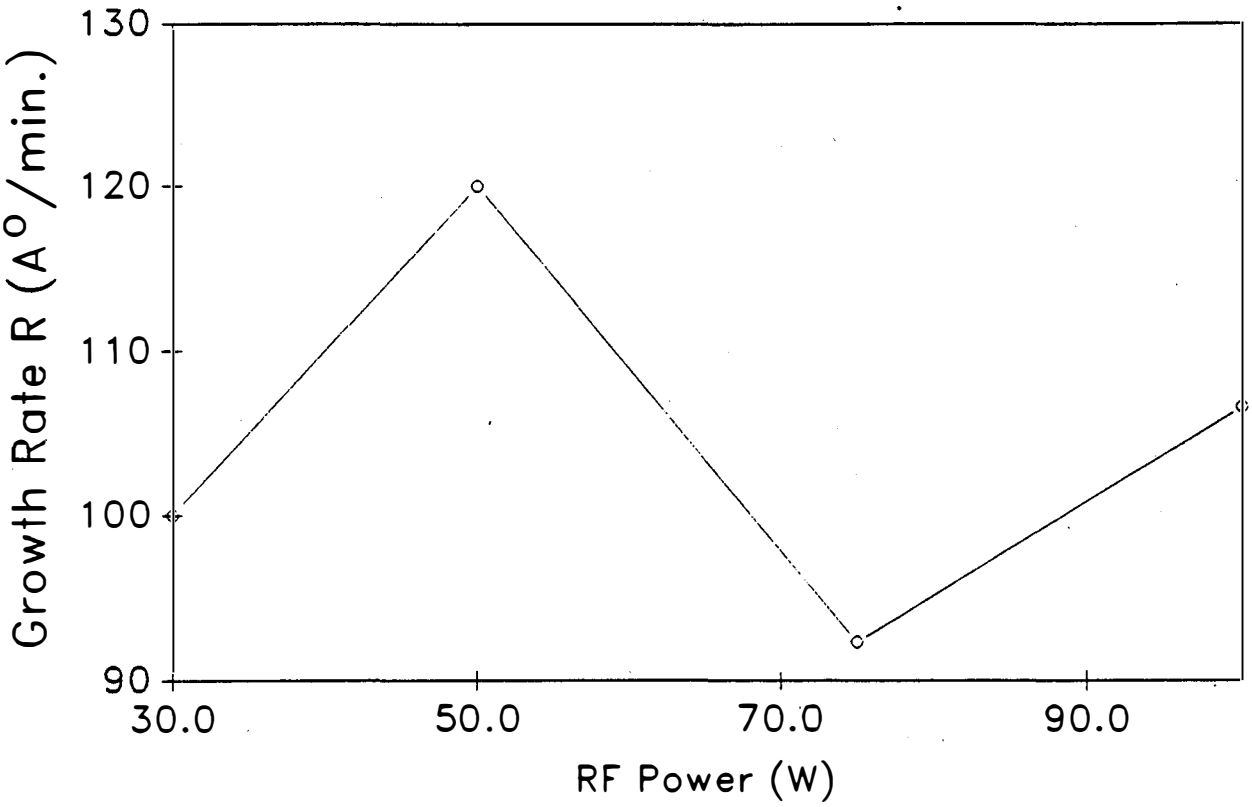

Fig.9 RF power effect on film growth rate.

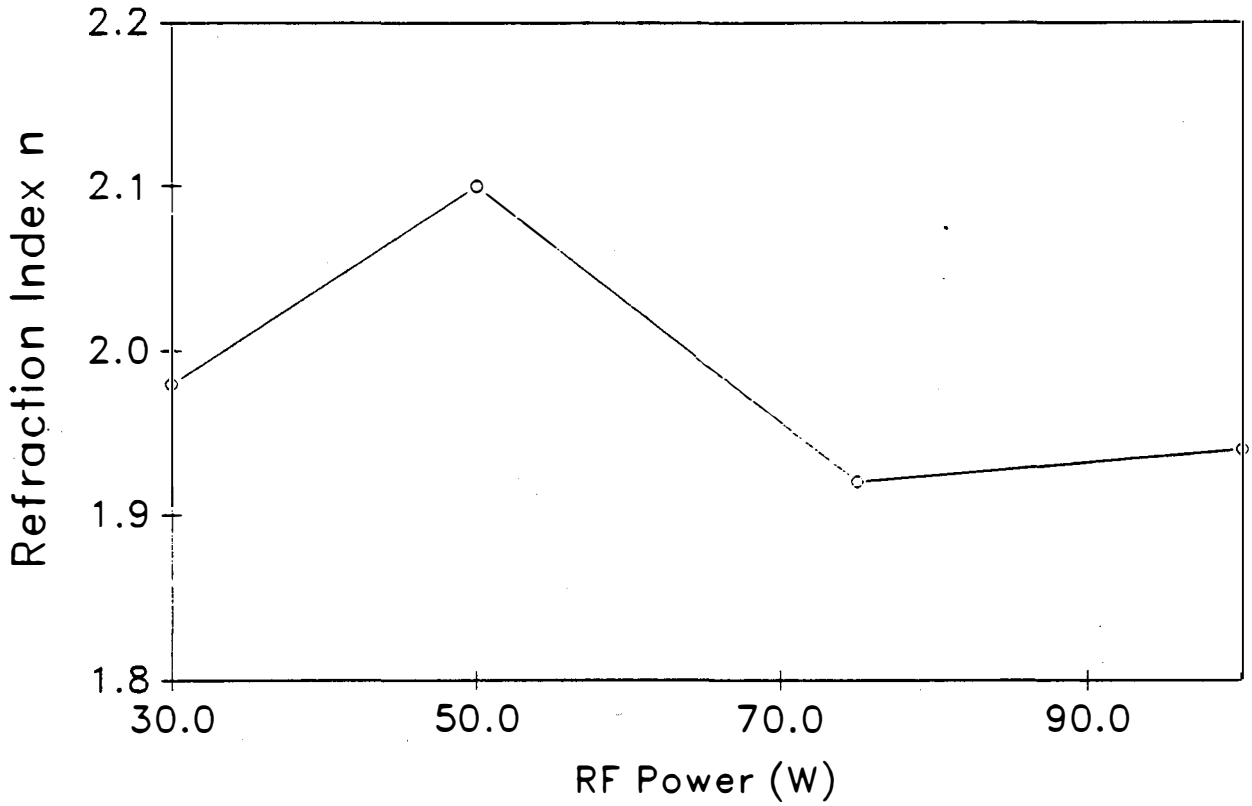

Fig.10 RF power effect on refraction index.

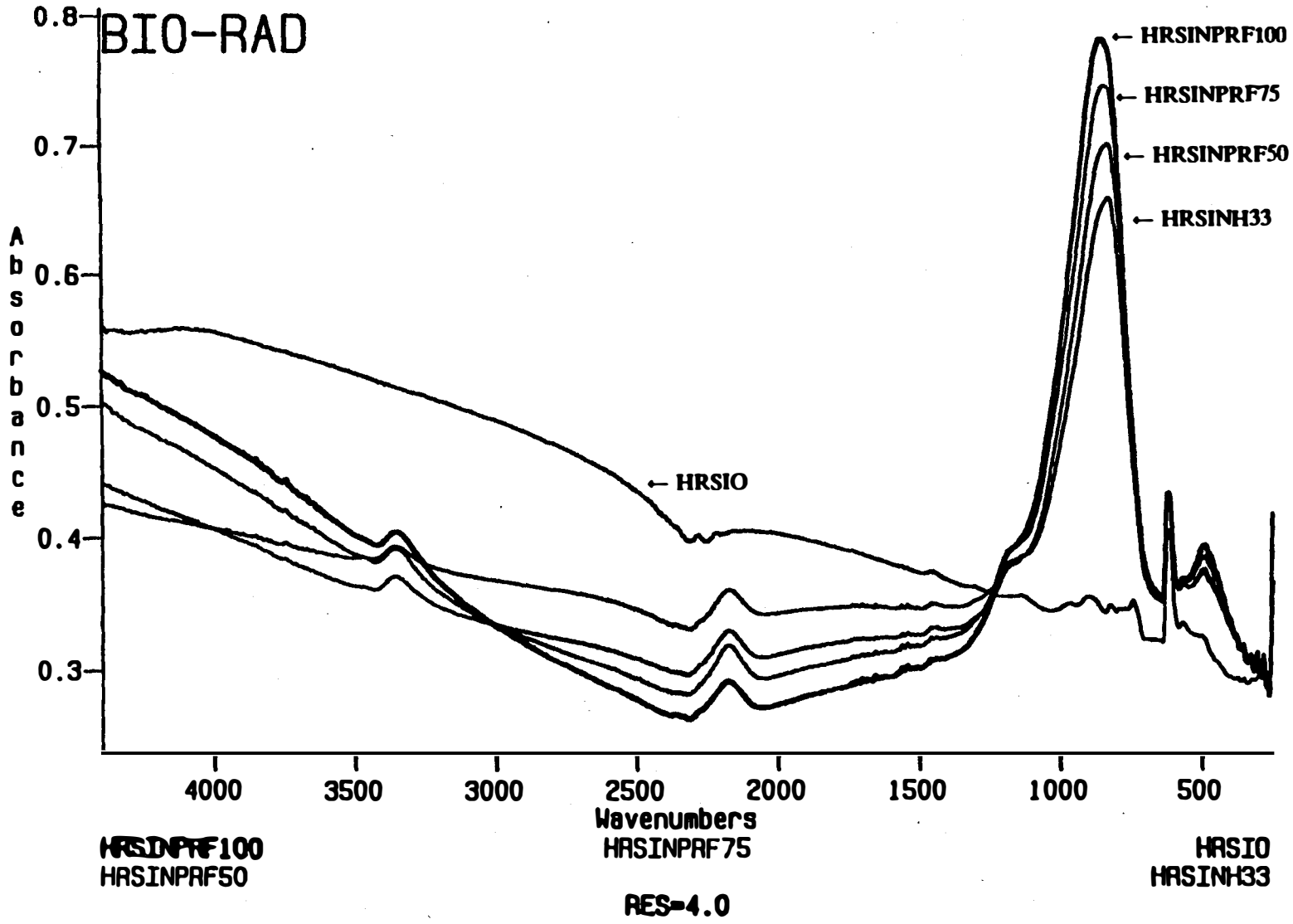

Fig.11 Infrared spectrum for different deposition rf power.

4. Fabrication of Polycrystalline Silicon Solar Cells

This section summarizes a solar cell run made on Osaka Titanium, EFG MOBIL, and single crystal FZ materials with Phosphorus diffusion on the front and Al diffusion on the back after process optimization of each step. The cell configuration for this specific run is shown in Figure and the corresponding process sequence is as follows:

1. Wafer Clean
2. Phos. Diffusion

   Solid source, 930° C, 30 min.

   Measured sheet resistance: 20 Ω/□
3. Etch Back

   100 Ω/□
4. Al Evaporation on the Back Side

   Thermal Evap.; thickness: 1.5 μm
5. Al Diffusion and Oxidation

   875° C, 10 min. O_2 , 30 min. N_2
6. Lift -off

   Ti/Ag 600/600 Å
7. Annealing

   Forming Gas 30 min. at 400° C
8. Electroplating

   Silver thickness; 4-5 μm

9. Mesa etch

10. AR Coating; Double layer

MgF_2: 1100 Å

ZnS : 500 Å

The results are summarized in the following table.

One Sun Polycrystalline and Single Crystal Cells tested at NREL

Cell ID	ρ (Ω.cm)	J_{sc}	V_{oc}	FF	EFF
OSAKA					
GT125#23	1.05	35.60	0.626	0.7921	17.7
GT125#43	1.05	35.16	0.623	0.7851	17.2
EFG MOBIL					
GT135#23	3.00	31.85	0.569	0.7800	14.1
GT135#22	3.00	31.02	0.567	0.7815	13.8
SINGLE CRYSTAL					
GT130#22	0.2	34.44	0.651	0.8040	18.1
GT130#11	0.2	34.39	0.653	0.8010	18.0

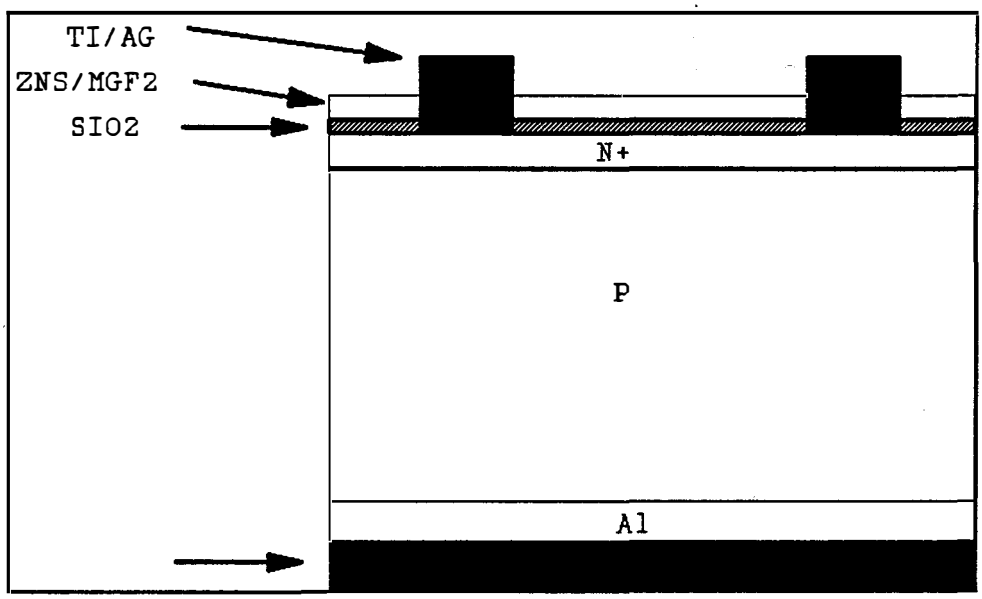

One Sun Polycrystalline Cell Structure

Georgia Inst Tech Multi-Si Global

Sample: GIT125#23 Temperature = 25.0°C

Jan. 29, 1992 3:12 pm Area = 1.000 cm²

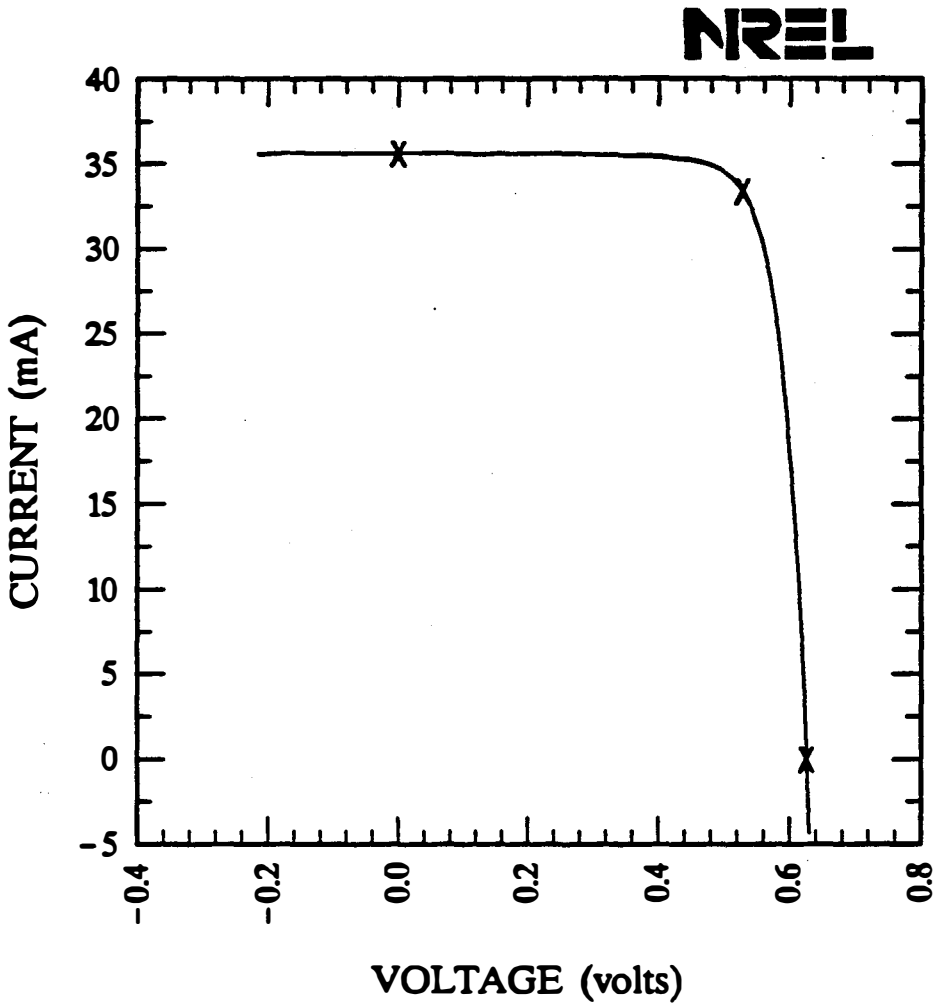

V_{oc} = 0.6259 volts	I_{sc} = 35.60 mA
J_{sc} = 35.60 mA/cm²	P_{max} = 17.65 mW
Fill factor = 79.21 %	I_{max} = 33.40 mA
Efficiency = 17.7 %	V_{max} = 0.5284 V

5. Fabrication of Single Crystal Silicon Solar Cells for Optical Deposition of Al at NREL.

This section summarizes cell runs made on low resistivity (0.2 Ω-cm) FZ Wacker materials. A process sequences was designed to fabricate N^+PP^+ solar cells for optical Al deposition purpose on finished solar cells. These solar cells can be used to test the finished cells after Al deposition. Detail of process sequences is given in Tables 5-I.

The cells fabricated with process sequence given in table 5-I were tested at NREL and the results are summarized in Table 5-II. Figures 5-1 shows the cells made using the given process sequence.

Table 5-I PROCESS SEQUENCE

STEPS

1. Wafer selection
   0.2 Ω-cm
   300 μm
   (100) P-TYPE

2. Oxidation at 1050 °C for two hours

3. Patterning and texturing

4. Oxidation at 1050 °C for two hours

5. Patterning and phosphorus diffusion
   Solid source, 930 °C, 40 minutes
   20 Ω / □

6. Patterning and phosphorus diffusion
   solid source, 900 °C, 15 minutes
   100 Ω / □ field diffusion

7. Oxide passivation
   1000 °C for 65 minutes
   FGA for 30 minutes

8. Al evaporation
   Evaporate 1-1.5 μm Al on half of the back side
   Al diffusion at 750°C

9. Back and top contact metal and lift off
   Ti/Ag 500/500 Å

10. Ag plating

11. Sinter
    Forming gas at 400°C for 30 minutes

Table 5-II One sun FZ solar cell parameters using process given in table 5-I tested at NREL.

Cell ID	J_{sc}	V_{oc}	FF	EFF%
OP-1-1	37.01	0.650	0.763	18.3
OP-1-2	36.56	0.649	0.764	18.1
OP-1-3	36.13	0.645	0.752	17.5

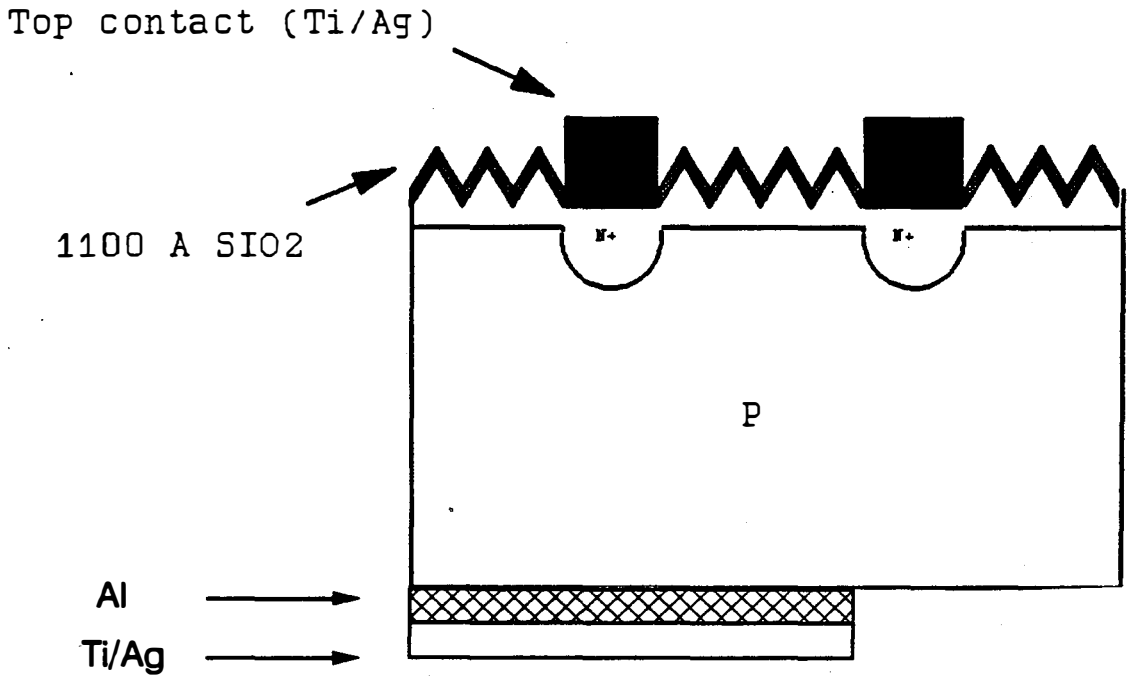

Figure 5-1 Solar cell designed to test optical deposition of Al at NREL.

6. SUMMARY

A combination of grain boundary model and solar cell modelling is used to quantify the effect of illumination level on diffusion length and efficiency of polysilicon cells. The results shows that the higher illumination level (> 10 Suns) reduces the grain boundary potential, enhances the diffusion length, and thereby reduces the gap in cell's efficiencies between single- and poly-crystalline silicon materials.

Systematic study of the effects of deposition temperature, reactant ratio and rf power on refraction index, growth rate, and Si-H, N-H, Si-N absorptions has been conducted. The results show that refractive index of SiN film can be adjusted in the range of 3.5 to 2.0 by controlling substrate temperature, rf power, and gas flow ratio NH_3/SiH_4. Hydrogen contents in SiN films can be monitored by Si-H and N-H vibration modes of the FTIR absorption spectrum. FTIR studies indicated that hydrogen content in SiN films is strong function of deposition temperature, and it increases with decreasing of the temperature. The results of refractive index and hydrogen concentration in this study should help in finding an optimum deposition condition for SiN film used for silicon solar cell application. Experiments are now in progress to deposit these films on solar cells. Solar cell performance is being monitored and analyzed to separate and quantify the AR coating and defect passivation effects of PECVD SiN films. Preliminary cell results show that PECVD SiN/SiO_2 double layer AR coating gives more than 50 % enhancement in J_{sc} for both single crystal cell and polycrystal cell, and single crystal cell efficiency went up from 10.58 % to 18.53 % and polycrystal cell went up from 8.2 % to 14.52 %.

Finally attempts were made to achieve high efficiency polycrystalline cells by a combination of gettering and passivation. Optimized phosphorous diffusion on the front and aluminum treatment at the back were used for gettering which resulted in record 17.7

7. REFERENCES

1. C.T. Ho, R.O. Bell, F.V. Wald, Applied Phys. Letters, 31 (7),463 (1977).

2. P.A. Basore, D.T. Rover, A.W. Smith, Proc. of 20th IEEE Photovoltaic Specialists Conf., 389- 396, (1988).

3. T.K. Kamins, J. Appl. Phys. 42, 4357 (1971).

4. J.Y.W. Seto, J. Appl. Phys. 46, 5247 (1975).

5. C.H. Seager and T.G. Castner, J. Appl. Phys., 49, 3879 (1978).

6. G. Baccarani, B. Ricco and G. Spadini, J. Appl. Phys. 49, 5565 (1980).

7. J. Martinez and J. Piqueras, Solid-State Electron 23, 297 (1980).

8. N.C.C. Lu, L. Gerzberg, C.Y. Lu and J.D. Meindl, IEEE Trans. Electron Devices, ED-28, 818 (1981).

9. S. Noor and C.E. Rogers, Solid-State Electron, 31, 1157 (1988).

10. D.P. Joshi and R.S. Srivastava, J. Appl. Phys. 59, 2549 (1986).

11. Z. Chen and L.C. Burton, 21st IEEE Photovoltaic Spec. Conf., p. 731 (1990).

12. J.G. Fossum, Solid-State Electron, 19, 269, (1976).

13. Z. Chen, L.C. Burton, Phys. Stat. Sol. (a) 122, 361 (1990).

14. H.C. Heieh, C. Hu and C.I. Drowley, IEEE Trans. Electron Devices, ED-27, 883 (1980).

15. G. Mathian, H. Amzil, M. Zehhaf, J.P. Crest, E. Psaila and S. Martinuzzi, Solid-State Electron, 21, 1045 (1978).

16. S.M. Sze, Semiconductor Devices,John Wiley & Sons,(1985)

17. P.P Michiels, etc. 21st PVSC, p638, 1990.

18. M.Iemiti, J. Gervais, and S. Martinuzzi, 22nd PVSC, 1991.

19. J.C. Muller, etc., 22nd PVSC, 1991.

20. K.Shirasawa, etc., Technical Digest of Internal PVSEC-3, Tokyo, Japan, B-IP-8, 1987.

21. Ram Kisshore, S.N.Singh, B.K. Das, 6th PVSEC, New Delhi, India, p249,1992.

22. S. Narayanan, S.Ronein, J.Wohlgemuth, 6th, PVSEC, New Delhi, India, p133, 1992.

23. W.A. Lanford, J. Appl.Phys. 49(4),1978.

24. R.Fessenden, J.Org. chem. 25 2191,1960.

25. W.R. Knolle and J.W. Osenbach, J.Appl.Phys. 58(3),1985.

8. ACKNOWLEDGEMENTS

Authors would like to thank Dr. B.L. Sopori of SERI and Dr. James Gee of Sandia National Laboratory for technical discussions, Drs. Keneko of Osaka Titanium and Mohen Narayanan of Solarex for cast silicon wafers, Drs. R.O. Bell and J.P. Kalejs of Mobil Solar for the EFG material and discussions.